Published in final edited form as:
Cancer Discov. 2013 June ; 3(6): 648–657. doi:10.1158/2159-8290.CD-13-0092.

Succinate Dehydrogenase Mutation Underlies Global Epigenomic Divergence in Gastrointestinal Stromal Tumor

J. Keith Killian[1], **Su Young Kim**[1], **Markku Miettinen**[1], **Carly Smith**[1], **Maria Merino**[1], **Maria Tsokos**[1], **Martha Quezado**[1], **William I. Smith Jr**[2], **Mona S. Jahromi**[4], **Paraskevi Xekouki**[3], **Eva Szarek**[3], **Robert L. Walker**[1], **Jerzy Lasota**[1], **Mark Raffeld**[1], **Brandy Klotzle**[5], **Zengfeng Wang**[1], **Laura Jones**[1], **Yuelin Zhu**[1], **Yonghong Wang**[1], **Joshua J. Waterfall**[1], **Maureen J. O'Sullivan**[7], **Marina Bibikova**[5], **Karel Pacak**[3], **Constantine Stratakis**[3], **Katherine A. Janeway**[6], **Joshua D. Schiffman**[4], **Jian-Bing Fan**[5], **Lee Helman**[1], and **Paul S. Meltzer**[1]

[1]National Cancer Institute-Center for Cancer Research [2]Suburban Hospital [3]Eunice Kennedy Shriver NICHD, Bethesda, Maryland [4]University of Utah, Salt Lake City, Utah [5]Illumina, Inc., San Diego, California [6]Dana Farber Cancer Institute, Boston, Massachusetts [7]Our Lady's Children's Hospital, Dublin, Ireland

Abstract

Gastrointestinal stromal tumors (GIST) harbor driver mutations of signal transduction kinases such as KIT, or, alternatively, manifest loss-of-function defects in the mitochondrial succinate dehydrogenase (SDH) complex, a component of the Krebs cycle and electron transport chain. We have uncovered a striking divergence between the DNA methylation profiles of SDH-deficient GIST ($n = 24$) versus KIT tyrosine kinase pathway–mutated GIST ($n = 39$). Infinium 450K methylation array analysis of formalin-fixed paraffin-embedded tissues disclosed an order of magnitude greater genomic hypermethylation relative to SDH-deficient GIST versus the *KIT*-mutant group (84.9 K vs. 8.4 K targets). Epigenomic divergence was further found among *SDH*-mutant paraganglioma/pheochromocytoma ($n = 29$), a developmentally distinct SDH-deficient

Corresponding Author: Paul S. Meltzer, Genetics Branch, National Cancer Institute, 37 Convent Drive MSC 4265, Bethesda, MD 20892-4265. Phone: 301-496-5266; Fax: 301-402-3241; pmeltzer@mail.nih.gov.

Note: Supplementary data for this article are available at Cancer Discovery Online (http://cancerdiscovery.aacrjournals.org/).

Disclosure of Potential Conflicts of Interest

B. Klotzle and M. Bibikova are employees of Illumina, Inc. J.D. Schiffman is a consultant/advisory board member of Affymetrix, Inc. J.-B. Fan is an employee of Illumina, Inc. No potential conflicts of interest were disclosed by the other authors.

Authors' Contributions

Conception and design: J.K. Killian, M. Miettinen, C.A. Stratakis, L.J. Helman, P.S. Meltzer
Development of methodology: J.K. Killian, M. Miettinen, R. Walker, Z. Wang, J.-B. Fan
Acquisition of data (provided animals, acquired and managed patients, provided facilities, etc.): S.Y. Kim, M. Miettinen, C. Smith, M. Merino, M. Tsokos, M. Quezado, W.I. Smith Jr, M.S. Jahromi, E. Szarek, J. Lasota, B. Klotzle, Z. Wang, L. Jones, M. Bibikova, K. Pacak, K.A. Janeway, J.D. Schiffman, J.-B. Fan, L.J. Helman, P.S. Meltzer
Analysis and interpretation of data (e.g., statistical analysis, biostatistics, computational analysis): J.K. Killian, M. Miettinen, M. Quezado, M.S. Jahromi, J. Lasota, Y.J. Zhu, Y. Wang, J. Waterfall, C.A. Stratakis, K.A. Janeway, J.D. Schiffman, P.S. Meltzer
Writing, review, and/or revision of the manuscript: J.K. Killian, S.Y. Kim, M. Miettinen, M. Tsokos, M. Quezado, M.S. Jahromi, E. Szarek, J. Lasota, M. Raffeld, J. Waterfall, M.J. O'Sullivan, K. Pacak, K.A. Janeway, J.D. Schiffman, L.J. Helman, P.S. Meltzer
Administrative, technical, or material support (i.e., reporting or organizing data, constructing databases): C. Smith, M.S. Jahromi, P. Xekouki, J. Lasota, M. Bibikova
Study supervision: C.A. Stratakis, P.S. Meltzer

tumor system. Comparison of *SDH* -mutant GIST with isocitrate dehydrogenase -mutant glioma, another Krebs cycle–defective tumor type, revealed comparable measures of global hypo- and hypermethylation. These data expose a vital connection between succinate metabolism and genomic DNA methylation during tumorigenesis, and generally implicate the mitochondrial Krebs cycle in nuclear epigenomic maintenance.

SIGNIFICANCE—This study shows that SDH deficiency underlies pervasive DNA hypermethylation in multiple tumor lineages, generally defining the Krebs cycle as mitochondrial custodian of the methylome. We propose that this phenomenon may result from a failure of maintenance CpG demethylation, secondary to inhibition of the TET 5-methylcytosine dioxgenase demethylation pathway, by inhibitory metabolites that accumulate in tumors with Krebs cycle dysfunction.

INTRODUCTION

DNA methylation profiles have been shown to carry clinical predictive and/or prognostic value for multiple tumor types, and thus epigenotype–phenotype correlation is a powerful approach in cancer discovery and translational research. Recently, a clinically relevant oncogenotype–epigenotype correspondence has been established for some tumor mutation subtypes, and has provided novel insight into the mechanistic basis of cancer epigenomic reprogramming (1–3).

Gastrointestinal stromal tumor (GIST), the most common mesenchymal tumor of the gastrointestinal tract, is alternatively driven by mutant cell surface KIT kinase pathway hyperactivation or mitochondrial metabolic derangement due to frequent mutation of succinate dehydrogenase complex (SDH) subunit genes *SDHA*, *SDHB*, *SDHC*, or *SDHD* (4–7). The distinction is important clinically because oncogenic *KIT* mutations are “actionable” and may be targeted by therapy directed at mutant cell surface tyrosine kinase receptors (8). In contrast, the tumorigenic biochemis try of SDH deficiency stems from within the mitochondria. Normally, SDH converts succinate to fumarate in the Krebs/tricarboxylic acid cycle while providing electrons for oxidative phosphorylation in the inner mitochondrial membrane (9).

Tumor suppression by the SDH complex is mediated by regulation of the level of succinate. Succinate accumulation within SDH-deficient cells inhibits α-ketoglutarate (α-KG)-dependent dioxygenase-catalyzed reactions that generate succinate and CO_2 as byproducts. For instance, elevation of succinate levels unblocks the hypoxia-inducible factor (HIF) angiogenic pathway by inhibiting HIF prolyl hydroxylation by prolyl hydroxylase (PHD; refs. 8–10). Other dioxygenases, including some required for chromatin maintenance and DNA methylome stability, have also been reported to be affected by such a succinate product inhibition mechanism (10). For example, succinate accumulation in SDH deficiency was shown to be inhibitory for histone demethylation by JMJD3 (11). And more recently, SDH knockdown was found to elevate intracellular succinate levels and the succinate/α-KG ratio, which in turn was shown to antagonize TET2 dioxygenase-catalyzed oxidation of 5-methylcytosine (5-mC) to 5-hydroxymethylcytosine (5-hmC), i.e., the initial step in the DNA demethylation pathway (12). Currently, the effects of SDH deficiency on tumor tissue

DNA methylation programming are not known, but based on these prior studies, altered profiles may be hypothesized.

Thus, beyond an important clinical distinction, the oncogenotype duality of GIST tumor subtypes suggests an elegant natural model in which to evaluate for epigenotype correlation, and further explore the role of mitochondrial processes in epigenomic programming. In the current study, we analyze the DNA methylome profiles of GIST tumors as a function of SDH- versus kinase- driver-mutation subclass. We then compare the methylomes of multiple Krebs cycle–mutant tumors across disparate developmental lineages including GIST, paraganglioma, pheochromocytoma, and glioma.

RESULTS

GIST, Comparison Tumors, and Normal Reference Samples

Included in the GoldenGate methylation analysis were 186 samples: 63 GIST (24 *SDH*-mutant and 39 KIT kinase pathway-mutant); 21 glioma (7 *IDH1*-mutant and 14 *IDH1* R132 wild-type); 29 paraganglioma/pheochromocytoma (20 *SDH*-mutant and 9 wild-type); and 73 normal reference tissues including gastrointestinal muscularis mucosa, gastric mucosa, neuronal tissue, glial tissue, adrenal gland, and lymphoid tissue (Figs. 1–4; Supplementary Table S1).

Bimodal GIST Methylation Programming

Target methylation profiles of GIST samples fit a strongly bimodal distribution (Fig. 1B). *SDH* mutation versus kinase pathway mutation status segregated perfectly with the 2 methylation subclasses (Fig. 1B). Also, SDH complex deficiency as determined by immunohistochemistry (IHC) segregated perfectly with both *SDH* mutation and methylation subclasses, as all *SDH*-mutant tumors, but no kinase pathway mutants, were SDH-deficient by IHC.

Methyl Divergence of *SDH*-Mutant GIST

To compare epigenomic divergence from baseline of the 2 SDH subclasses, we analyzed the relatedness of subclass methylation profile to those of multiple anatomically relevant normal tissues (Fig. 1A and C; Supplementary Table S2; refs. 13, 14). GIST is postulated to derive from the lineage of interstitial cell of Cajal (ICC), a mesodermal cell resident of the gastrointestinal tract involved in peristalsis and with both neuronal and mesenchymal characteristics (15, 16). Thus, neuronal cells and gut muscularis (Fig. 1A) were selected for the relatedness comparison. Also included were gut mucosa and lymphoid tissue, potential constituents of GIST specimens.

Unsupervised principal component analysis (PCA) and hierarchical clustering showed that the kinase-mutant GIST methylome signature most closely resembles that of all evaluated normal tissues, particularly muscularis tissue (Fig. 1C). In contrast, the *SDH* -mutant subclass comprised a distant out-group to all tissues (Fig. 1C). The marked divergence of the SDH-deficient methylation profile from multiple normal references argues against a purely clonal enrichment for the epigenome of a normal cell precursor population in normal gut,

and instead supports a divergence during tumorigenesis. Thus, the kinase-mutant and SDH-deficient GIST methylation subclasses were respectively termed methyl-centrist and methyl-divergent.

We subsequently quantified the relative contributions of hypo- and hypermethylations to the aberrant methylation profiles of *SDH* - versus kinase-mutant GIST (Fig. 2). Interestingly, we observed a comparable number of significant CpG target hypomethylations in both subclasses: 209 and 203, respectively; in contrast, we observed 457 significant hypermethylations in the *SDH* mutants versus only 19 among KIT pathway mutants (Fig. 2A–C; Supplementary Table S2). Overall, there is a comparable and substantial hypomethylation fraction in both oncogenotypes, but significantly greater genomic hypermethylation in *SDH* mutants.

The 450 K Infinium Methylation array platform, with 300 times the coverage of GoldenGate arrays, confirmed these results (Fig. 2D–F). First, the 450 K arrays revealed sizable and comparable hypomethylation activities in both SDH-deficient/ methyl-divergent and kinase-mutant/methyl-centrist GIST: 66.7 K and 71.6 K CpG targets, respectively. Second, the high-density arrays uncovered an order of magnitude greater number of hypermethylated differentially methylated CpG targets (DMT) between methyl-divergent and -centrist GIST subclasses: 84.9 K versus 8.4 K.

Among SDH-deficient tumors, there was proportionate hypermethylation of CpG-island (CGI) and non-CGI genomic domains (Fig. 2G); similarly, other genomic motifs, including gene promoters, bodies, and enhancers, were hypermethylated in proportion to their representation on the arrays (Fig. 2G). In contrast, this analysis did positively identify significant enrichment for DNase hypersensitive sites (DHS) among the methyl-divergent GIST DMT (Fig. 2G). Thus, the underlying process of widespread hypermethylation in SDH deficiency cannot be satisfactorily characterized as CpG-island methylator specific. In addition, differential methylation in these tumors is not randomly distributed, as evidenced by the large numbers of significant, recurrent hypo- and hyper-methylated genomic targets (66.7 K and 84.9 K targets, respectively, Supplementary Table S3), principal component uniformity among samples, hierarchical clustering (Fig. 2D and E), and significant enrichment for DHS (Fig. 2G).

Overall, the primary distinction observed by methylation microarray between *SDH*- and kinase pathway–mutant GIST was marked hypermethylation in the former. Neither subclass showed a significant bias toward CGI methylation as a fraction of total hypermethylation (Fig. 2G).

Loss of 5-hmC in Methyl-Divergent GIST

Mechanistically, accumulation of cytosine 5-methylation in methyl-divergent tumors may arise from *de novo* methylation and/or failed maintenance demethylation. It has been previously reported that elevated intracellular succinate levels result from SDH deficiency and are toxic for the dioxygenase TET2, an enzyme required to catalyze DNA demethylation by conversion of 5-mC to 5-hmC. Thus, GIST tumors were scored for loss of 5-hmC by immunohistochemistry. Sixteen of 24 methyl-divergent versus 1 of 12 methyl-

centrist tumors showed loss of 5-hmC ($P = 0.001$). Thus, the finding of significant deficiency of 5-hmC in *SDH*-null GIST (Fig. 2H) is consistent with a failure in TET2 maintenance demethylation in SDH-deficient GIST. This potential connection in GIST between succinate accumulation, TET inhibition, and loss of 5-hmC is supported by the recent finding in melanoma that downregulation of TET family proteins leads to loss of 5-hmC (17).

Genomic Stability of Methyl-Divergent GIST

We further evaluated the genomic copy number landscape of GIST for ties to the identified bimodal epigenomic divergence. The genomes of *KIT*-mutant/methyl-centrist GIST samples featured numerous and recurrent copy number aberrations, including gains and losses of multiple chromosome arms similar to most types of cancer (18) and other published reports of GIST (refs. 19, 20; Fig. 1B and Supplementary Fig. S1). In contrast, methyl-divergent GIST samples had remarkably stable genomes, with either no copy number changes or ≤2 chromosome arm copy number changes (Fig. 1B and Supplementary Fig. S1) often limited to a single somatic loss on 1p or 5p overlying germline *SDHB* or *SDHA* mutation. Thus, a highly altered epigenome is a unifying feature of SDH-deficient GIST, and in some cases may be the only identifiable molecular aberration. No samples had both a normal genome and a normal methylome, and overall we observed an inverse correlation between karyotypic aberration and epigenomic divergence in GIST samples (Fig. 1B).

Methyl Divergence in SDH-Deficient Paraganglioma and Pheochromocytoma

We next sought to further validate and test the generality of the link between *SDH* mutation and methyl-divergence in tumorigenesis. As a model system, we analyzed other naturally occurring human SDH-deficient tumor tissues, in particular *SDH*-mutant hereditary paraganglioma and pheochromocytoma (PGLs/Pheos). As is the case with GIST, a subset of PGLs/Pheos occur in the setting of germline *SDH* mutation followed by a somatic second hit, thereby creating a genetic and functional *SDH*-null tumor. In contrast with the mesenchymal lineage of GIST, PGLs/Pheos are neuroendocrine tumors of neural crest embryonic origin that arise in multiple anatomic sites outside the gut. We determined the methyl-divergence status for PGLs/Pheos based on comparison with the adrenal reference tissue, including microdissected adrenal medulla, the postulated lineage of origin for Pheo (Fig. 3A). GoldenGate DNA methylation profiles from 29 PGLs/Pheos showed an elevated total number of target hypermethylations in the *SDH* -mutant versus -wild-type subgroup (177 targets versus 49 targets; Fig. 3B; Supplementary Table S2). Moreover, as in GIST, there is an elevated ratio of hyper- to hypomethylated targets in the *SDH*-mutant group, whereas in the *SDH*-wild-type group, hypermethylations are only a fraction of hypomethylations (Fig. 3C–F). Thus, human SDH-deficient tumors from multiple anatomic origins, including stomach, adrenal, and carotid body and other paraganglia, manifest oncogenotype-dependent methyl-divergent profiles.

Comparison of SDH- and IDH-Defective Tumors

Upstream of SDH in the Krebs cycle, isocitrate dehydrogenase (IDH) catalyzes the oxidative decarboxylation of isocitrate, producing α-KG and CO_2. Mutation of *IDH* genes is coupled

with heightened genomic methylation in several cancers. As postulated for elevated succinate levels stemming from SDH deficiency, the result of *IDH* mutation is accumulation of a metabolite that is inhibitory for TET family dioxygenase-mediated DNA demethylation. Using the GoldenGate methylation assay, we compared the epigenomic profiles of *SDH*-mutant GIST with those of *IDH1*-mutant glial neoplasms (i.e., gliomas). Normal brain glial tissue served as the differential methylation reference tissue for glioma (Fig. 4A–C). We identified 388 and 140 hyper- and hypomethylations in *IDH1*-mutant gliomas, compared with 457 and 209 in *SDH*-mutant GIST (Fig. 4; Supplementary Table S2). Thus, *IDH1*-mutant glioma and *SDH* -mutant GIST epigenomes have comparable proportions of hyper- and hypomethylation.

Subsequently, we conducted combined analysis on all the tumors in the study. Unsupervised hierarchical clustering assorted the gliomas, GIST, paragangliomas, and pheochromocytomas, not according to anatomic site of origin, but instead according to presence or absence of a Krebs cycle mutation (Fig. 4D); the heatmap further displays that hypermethylated targets in *SDH* -mutant GIST are similarly hyper-methylated in other Krebs cycle–mutant tumors. Next, the PCA analysis showed the Krebs cycle–mutant tumors to lie along a shared principal axis orthogonal to the nonmutants, which more closely clustered with the normal tissues (Fig. 4E). Taken together, these data identify epigenomic homology of tumors from 4 divergent developmental lineages that have in common a mutation of a Krebs cycle enzyme.

DISCUSSION

In this study, we have found a striking correspondence between GIST oncogenotype and epigenotype, as evidenced by marked methyl-divergence of *SDH* mutants. Although impaired SDH function has previously been tied to tumorigenesis (21) and chromatin modification (11), epigenomic profiling of SDH-deficient versus kinase pathway–mutant tumors has not been reported.

One of the first described targets of pathologic succinate accumulation in cancer was the HIF-1 PHD, the inhibition of which leads to increased HIF-1α activity and resultant tumorigenesis (22). Beyond unfettering HIF-1–mediated processes, succinate accumulation has been found to inhibit additional α-KG–dependent processes that generate succinate and CO_2 as byproducts (10). For example, DNA demethylation through the oxidation of 5-mC to 5-hmC depends upon the dioxygenase TET2, and is inhibited by intracellular succinate accumulation; in the setting of SDH deficiency, tumors may be expected to accumulate 5-mC or lose 5-hmC, analogous to epigenotype profiles in tumors harboring *IDH* mutations or TET protein downregulation, respectively.

Thus, our results suggest a mechanism for cancer-related DNA hypermethylation in SDH-deficient GIST that may be analogous to that proposed for *IDH* mutations in gliomas and leukemia. Rather than unscheduled *de novo* methyltransferase activity, we propose that the hypermethylation phenomenon in this class of tumors may involve failure of maintenance DNA demethylation. Consistent with this idea, we found that *SDH*-mutant Pgl/Pheo and GIST have similar proportions of hyper- and hypomethylated targets.

Importantly, we found that the methyl-divergence process is not random, as we uncovered tens of thousands of significant, recurrent hypermethylations and hypomethylations. Within the hypermethylated genomic compartment, we found DHS to be significantly enriched. It is possible that the identified changes define a succinate-sensitive hypermethylation genomic space in the GIST lineage. With this report, the methyl-divergence landscape of GIST tumors is now well characterized and clearly connected to the oncogenotype. Although the consequences of this altered epigenetic state for tumor cell behavior remain uncertain and merit further exploration, the widespread perturbation that we have observed is unlikely to be phenotypically neutral. Our finding that younger patients with GIST with genome copy number-stable tumors have such dramatic epigenomic reprogramming seems to discount relative contributions from age-related epimutation and potential genomic damage from reactive oxygen species. The epigenomic similarities of diverse Krebs cycle–mutant tumors support the idea of a shared etiology stemming from their metabolite profiles. Thus, the current work definitively links SDH deficiency to pervasive DNA hypermethylation and generally implicates the Krebs cycle as mitochondrial custodian of the methylome.

METHODS

Tissue Specimens

Archival formalin-fixed paraffin-embedded (FFPE) tumor and reference tissues were provided by the Pediatric and Wildtype GIST Clinic (http://www.pediatricgist.cancer.gov/) at the NIH (6). Samples were reviewed by a pathologist, and regions of characteristic histomorphology were needle microdissected. Tissue cores were lysed and processed to yield genomic DNA (gDNA) as previously described (23, 24).

Immunophenotyping

SDHB and 5-hmC IHC staining and analysis were conducted in a central laboratory for uniformity of results. For SDHB, clone 21A11 (Abcam) was used at 1:1,000 dilution. For 5-hmC, polyclonal rabbit anti 5-hmC (Active Motif) was used at 1:2,000 dilution. IHC was conducted on a Bond-Max autostainer [Leica Microsystems with high pH antigen retrieval (AR2, pH 8.0)]. Loss of 5-hmC staining was defined as a ≥50% reduction in staining of tumor cell versus peritu-moral normal fibrovascular stroma.

Genomic Copy Number Analysis

Tumor gDNAs were analyzed for chromosomal copy number aberrations using a commercial 180 K-feature array comparative genomic hybridization (aCGH) assay (Agilent Inc.). Array fluorescence intensities were imported to Nexus 6.0 (Biodiscovery) and analyzed using standard segment gain/loss settings. Genomic copy number near normal is defined as ≤2 gross chromosome arm gains or losses; genomic copy number aberration is defined as ≥3 gross chromosome arm gains or losses. Representative aCGH results are displayed in Supplementary Fig. S1.

DNA Methylation Arrays

GoldenGate—gDNA was bisulfite converted and assayed using the GoldenGate Cancer Panel I methylation assay (Illumina, Inc.) as described previously (23, 25). Briefly, this

assay measures DNA methylation at 1536 distinct CpG targets distributed among 818 genes. Methylation β values were extracted from Cy3 and Cy5 signal intensities using BeadStudio software (Illumina, Inc.), and samples were excluded that did not pass array signal intensity controls. GoldenGate Methylation β data are provided in Supplementary Table S2. These methylation β data may also be retrieved from Gene Expression Omnibus (GEO), accession number GSE34387.

Infinium 450 K Methylation Assay for FFPE Samples—We used the EZ DNA Methylation kit (Cat# 5004, Zymo Research) for bisulfite conversion of gDNA extracted from FFPE samples. For optimized results, we used 250 ng of gDNA and followed the manufacturer's recommendations. Namely, gDNA was denatured by addition of NaOH-containing M-Dilution buffer and incubated for 15 minutes at 37°C. Freshly prepared CT-conversion reagent (Zymo Research) containing sodium bisulfite was added to the denatured DNA and samples were incubated for 16 hours at 50°C in a thermocycler and denatured every 60 minutes by heating to 95°C for 30 seconds. After bisulfite conversion, the DNA was bound to a Zymo-Spin I-96 Binding Plate, washed with M-Wash Buffer, and desulphonated on the binding plate using M-desulphonation reagent. The bisulfite-converted DNA was eluted from the plate wells in 10 μL elution buffer.

Bisulfite-converted DNA was restored using Infinium HD FFPE DNA Restore Kit (Cat#WG-321-1002, Illumina) following the manufacturer's recommendations. The process restores degraded FFPE DNA to a state that is amplifiable by the Infinium whole-genome amplification protocol. After DNA restoration, the Infinium Methylation assay was carried out as described previously (26). In brief, bisulfite converted and restored DNA (~8 μL) was used in the whole-genome amplification reaction. After amplification, the DNA was fragmented enzymatically, precipitated, and resuspended in hybridization buffer. All subsequent steps were conducted following the standard Infinium protocol (User Guide part #15019519 A). Fragmented DNA was dispensed onto the HumanMethylation450 BeadChips, and hybridization conducted in a hybridization oven for 20 hours. After hybridization, these arrays were processed through a primer extension and an IHC staining protocol to allow detection of a single-base extension reaction. Finally, BeadChips were coated and then imaged on an Illumina iScan. 450 K methylation array data are provided via GEO accession number GSE34387.

Mutation Identification

For GIST tumors, genomic DNA libraries were constructed and *SDHA*, *SDHB*, *SDHC*, *SDHD*, *KIT*, *BRAF*, *NF1*, and *PDGFRA* genes were sequenced using a custom capture assay as previously described (7). *IDH1* status of gliomas was determined by Sanger sequencing of the R132 codon. *SDH* status of Pgls and Pheos was annotated as previously determined clinically, and results validated as part of this study.

Methylation Data Analysis

Beta values were imported to Qlucore Omics Explorer (QOE v2.2). For unsupervised cluster analyses, autosomal targets were selected, and then variance and normalization settings were dynamically tuned to produce the representative PCA plots and heatmaps shown in figures.

For PCA plots, data normalization in QOE was set to mean = 0, var = 1; for 2-dimensional (2D) heatmaps, data normalization method in QOE is indicated by the green–red color scale in the figure. Statistical significance of target differential methylation between various comparison groups is $P < 0.05$ and group delta $\beta > 0.1$. In 450 K methylation GIST group comparisons, annotation as SDH-deficient/ mutant versus KIT kinase pathway–mutant was based firstly upon sequencing and secondly upon SDHB IHC for *SDH/KIT* wild-type samples.

Supplementary Material

Refer to Web version on PubMed Central for supplementary material.

Acknowledgments

Grant Support

This work was supported by grants from the Intramural Research Program of NIH, the National Cancer Institute, and the Center for Cancer Research.

References

1. Noushmehr H, Weisenberger DJ, Diefes K, Phillips HS, Pujara K, Berman BP, et al. Identification of a CpG island methylator phenotype that defines a distinct subgroup of glioma. Cancer Cell. 2010; 17:510–22. [PubMed: 20399149]
2. Figueroa ME, Abdel-Wahab O, Lu C, Ward PS, Patel J, Shih A, et al. Leukemic IDH1 and IDH2 mutations result in a hypermethylation phenotype, disrupt TET2 function, and impair hematopoietic differentiation. Cancer Cell. 2010; 18:553–67. [PubMed: 21130701]
3. Pansuriya TC, van Eijk R, d'Adamo P, van Ruler MA, Kuijjer ML, Oosting J, et al. Somatic mosaic IDH1 and IDH2 mutations are associated with enchondroma and spindle cell hemangioma in Ollier disease and Maffucci syndrome. Nat Genet. 2011; 43:1256–61. [PubMed: 22057234]
4. Hirota S, Isozaki K, Moriyama Y, Hashimoto K, Nishida T, Ishiguro S, et al. Gain-of-function mutations of c-kit in human gastrointestinal stromal tumors. Science. 1998; 279:577–80. [PubMed: 9438854]
5. Pantaleo MA, Astolfi A, Indio V, Moore R, Thiessen N, Heinrich MC, et al. SDHA loss-of-function mutations in KIT-PDGFRA wild-type gastrointestinal stromal tumors identified by massively parallel sequencing. J Natl Cancer Inst. 2011; 103:983–7. [PubMed: 21505157]
6. Janeway KA, Kim SY, Lodish M, Nose V, Rustin P, Gaal J, et al. Defects in succinate dehydrogenase in gastrointestinal stromal tumors lacking KIT and PDGFRA mutations. Proc Natl Acad Sci U S A. 2011; 108:314–8. [PubMed: 21173220]
7. Miettinen M, Killian JK, Wang ZF, Lasota J, Lau C, Jones L, et al. Immunohistochemical loss of succinate dehydrogenase subunit A (SDHA) in gastrointestinal stromal tumors (GISTs) signals SDHA germline mutation. Am J Surg Pathol. 2013; 37:234–40. [PubMed: 23282968]
8. Demetri GD, Benjamin RS, Blanke CD, Blay JY, Casali P, Choi H, et al. NCCN Task Force report: management of patients with gastrointestinal stromal tumor (GIST)–update of the NCCN clinical practice guidelines. J Natl Compr Canc Netw. 2007; 5:S1–29. quiz S30. [PubMed: 17624289]
9. Gottlieb E, Tomlinson IP. Mitochondrial tumour suppressors: a genetic and biochemical update. Nat Rev Cancer. 2005; 5:857–66. [PubMed: 16327764]
10. Frezza C, Pollard PJ, Gottlieb E. Inborn and acquired metabolic defects in cancer. J Mol Med. 2011; 89:213–20. [PubMed: 21301796]
11. Cervera AM, Bayley JP, Devilee P, McCreath KJ. Inhibition of succinate dehydrogenase dysregulates histone modification in mammalian cells. Mol Cancer. 2009; 8:89. [PubMed: 19849834]

12. Xiao M, Yang H, Xu W, Ma S, Lin H, Zhu H, et al. Inhibition of alpha-KG-dependent histone and DNA demethylases by fumarate and succinate that are accumulated in mutations of FH and SDH tumor suppressors. Genes Dev. 2012; 26:1326–38. [PubMed: 22677546]
13. Miettinen M, Lasota J. Gastrointestinal stromal tumors: review on morphology, molecular pathology, prognosis, and differential diagnosis. Arch Pathol Lab Med. 2006; 130:1466–78. [PubMed: 17090188]
14. Rosai J. Gastrointestinal stromal tumor and its mimics. Int J Surg Pathol. 2010; 18:79S–87S. [PubMed: 20484268]
15. Rosai J. GIST: an update. Int J Surg Pathol. 2003; 11:177–86. [PubMed: 12894349]
16. Min KW. Gastrointestinal stromal tumor: an ultrastructural investigation on regional differences with considerations on their histogenesis. Ultrastruct Pathol. 2010; 34:174–88. [PubMed: 20455665]
17. Lian CG, Xu Y, Ceol C, Wu F, Larson A, Dresser K, et al. Loss of 5-hydroxymethylcytosine is an epigenetic hallmark of melanoma. Cell. 2012; 150:1135–46. [PubMed: 22980977]
18. Beroukhim R, Mermel CH, Porter D, Wei G, Raychaudhuri S, Donovan J, et al. The landscape of somatic copy-number alteration across human cancers. Nature. 2010; 463:899–905. [PubMed: 20164920]
19. Belinsky MG, Skorobogatko YV, Rink L, Pei J, Cai KQ, Vanderveer LA, et al. High density DNA array analysis reveals distinct genomic profiles in a subset of gastrointestinal stromal tumors. Genes Chromosomes Cancer. 2009; 48:886–96. [PubMed: 19585585]
20. Astolfi A, Nannini M, Pantaleo MA, Di Battista M, Heinrich MC, Santini D, et al. A molecular portrait of gastrointestinal stromal tumors: an integrative analysis of gene expression profiling and high-resolution genomic copy number. Lab Invest. 2010; 90:1285–94. [PubMed: 20548289]
21. Selak MA, Armour SM, MacKenzie ED, Boulahbel H, Watson DG, Mansfield KD, et al. Succinate links TCA cycle dysfunction to oncogenesis by inhibiting HIF-alpha prolyl hydroxylase. Cancer Cell. 2005; 7:77–85. [PubMed: 15652751]
22. Denko NC. Hypoxia, HIF1 and glucose metabolism in the solid tumour. Nat Rev Cancer. 2008; 8:705–13. [PubMed: 19143055]
23. Killian JK, Bilke S, Davis S, Walker RL, Jaeger E, Killian MS, et al. A methyl-deviator epigenotype of estrogen receptor-positive breast carcinoma is associated with malignant biology. Am J Pathol. 2011; 179:55–65. [PubMed: 21641572]
24. Killian JK, Bilke S, Davis S, Walker RL, Killian MS, Jaeger EB, et al. Large-scale profiling of archival lymph nodes reveals pervasive remodeling of the follicular lymphoma methylome. Cancer Res. 2009; 69:758–64. [PubMed: 19155300]
25. Bibikova M, Fan JB. GoldenGate assay for DNA methylation profiling. Methods Mol Biol. 2009; 507:149–63. [PubMed: 18987813]
26. Bibikova M, Le J, Barnes B, Saedinia-Melnyk S, Zhou L, Shen R, et al. Genome-wide DNA methylation profiling using Infinium(R) assay. Epigenomics. 2009; 1:177–200. [PubMed: 22122642]

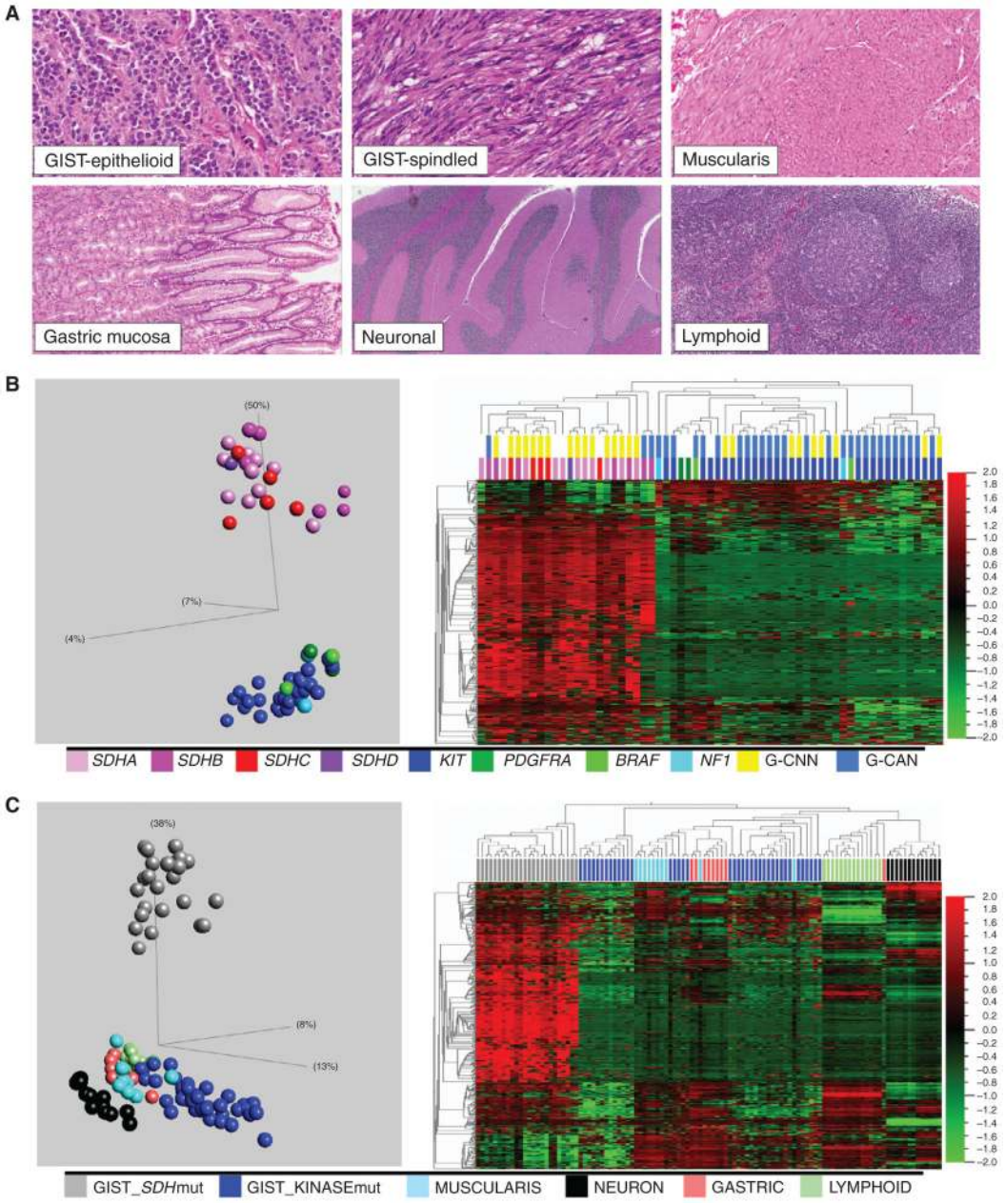

Figure 1.

A, Histomorphology of GISTs and comparison reference tissues. B, unsupervised PCA (left) and hierarchical clustering (right) sharply segregate *SDH*-mutant (*SDHA*, *B*, *C*, or *D*) and kinase-mutant (*KIT*, *PDGFRA*, *BRAF*, or *NF1*) GIST samples and reveal marked methylation in the *SDH* mutants. *SDH* mutation is also correlated with a nearly normal genomic copy number (G-CNN), whereas kinase mutation is correlated with a copy number abnormal genome (G-CAN). PCA and heatmaps were derived from the 476 autosomal targets remaining after a methylation β variance filter across the 63 GIST samples was set to 0.5. C, unsupervised PCA (left) and hierarchical clustering (right) of GISTs and normal reference tissues reveal distant divergence of *SDH*-mutant GIST. PCA and heatmaps were

derived from the 552 autosomal targets remaining after a methylation β variance filter across the 109 samples was set to 0.5. mut, mutant.

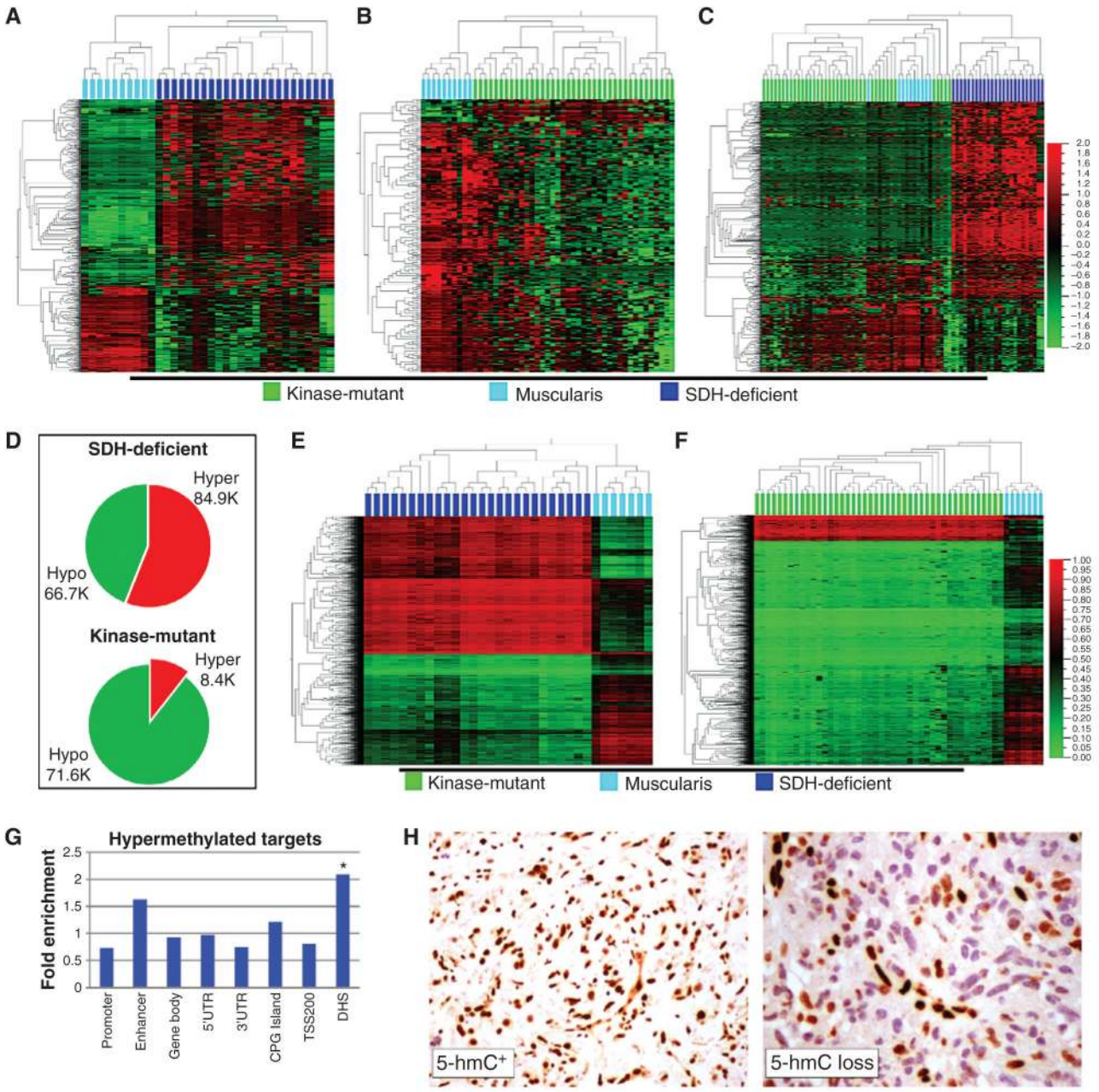

Figure 2.

Visual display of the proportions of hyper- and hypomethylated differentially methylated targets (DMT) relative to reference muscularis tissue in *SDH*- versus kinase-mutant GIST. **A,** 2-D hierarchical clustering of 24 *SDH*-mutant GIST (dark blue) and 10 reference muscularis samples (cyan); CpG targets (*y*-axis) are filtered for significant DMT between the 2 sample groups (GoldenGate methylation assay, group delta $\beta > 0.1$ and $P < 0.05$, $n =$ 666 targets). Of the DMT, 457 are hypermethylated and 209 are hypomethylated in *SDH*-mutant GIST. **B,** 2-D hierarchical clustering of 39 kinase-mutant GIST (green) and 10 reference baseline muscularis samples (cyan); CpG targets are filtered for significant DMT between the 2 sample groups (GoldenGate methylation assay, group delta $\beta > 0.1$ and $P <$

0.05, $n = 222$ targets). Of the DMT, 19 are hypermethylated, and 203 hypomethylated, in kinase-mutant GIST. **C,** 2-D hierarchical clustering of the union sets of all tissues [*SDH*-mutant GIST ($n = 24$), kinase-mutant GIST ($n = 39$), and reference muscularis ($n = 10$)] and DMT ($n = 748$ targets) from **A** and **B. D,** hyper- and hypomethylated DMT composition for SDH-deficient versus kinase-mutant GIST (Infinium 450 K methylation data). **E,** 2-D hierarchical clustering of SDH-deficient GIST ($n = 26$, dark blue) and reference muscularis tissues ($n = 7$, cyan) with Infinium 450 K methylation data; targets included on the *y*-axis are the top hyper- and hypomethylated DMT selected in proportion to their fraction of total DMT (DMT defined as group delta $\beta > 0.1$ and $P < 0.05$. Displayed on the heatmap is the union set of 1.7 K hyper- and 1.3 K hypomethylated DMT, which reflects their proportions of total DMT). **F,** 2-D hierarchical clustering of kinase-mutant GIST ($n = 44$, green) and reference muscularis tissues ($n = 7$, cyan) with Infinium 450 K methylation data; targets included on the *y*-axis are the top hyper- and hypomethylated DMT in proportion to their fraction of total DMT (DMT defined as group delta $\beta > 0.1$ and $P < 0.05$. Displayed on the heatmap is the union set of 0.3 K hyper- and 2.7 K hypomethylated DMT, which reflects their proportions of total DMT). **G,** fold enrichment of genomic annotations of hypermethylated targets in SDH-deficient GIST based on their proportion of all array targets. CpG target anatomic and functional annotations are according to the Illumina Infinium 450 K methylation assay manifest. * DNase hypersensitive site (DHS) is the only significantly enriched annotation ($P = 0.0022$) after Bonferroni correction. TSS200: within a distance of 200 bp of transcription start site. UTR, untranslated region. **H,** representative IHC results for 5-hmC$^+$ (left) and 5-hmC loss in GIST tumors (right). Sixteen of 24 methyl-divergent GIST had 5-hmC loss, versus 1 of 12 methyl-centrist.

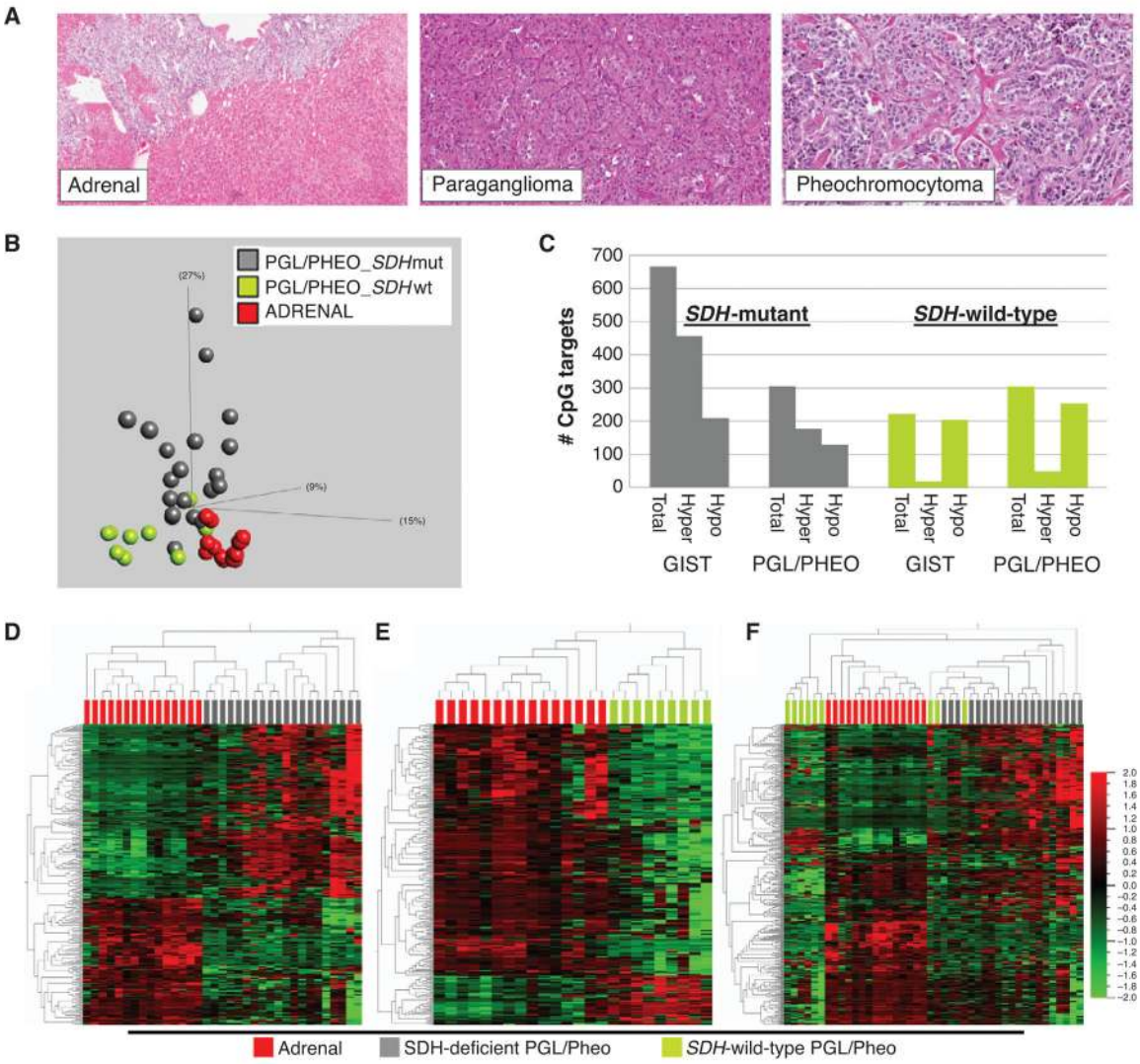

Figure 3.

Human SDH-deficient tumor genotype-epigenotype validation model. **A,** histomorphology of pheochromocytoma (pheo), paraganglioma (pgl), and comparison reference adrenal gland. **B,** left, PCA segregates pgl/pheo according to oncogenotype and reveals greater divergence from baseline adrenal for *SDH* mutants. The plot includes 20 *SDH*-mutant pgl/pheo, 9 SDH-wt pgl/pheo, and 15 reference adrenal specimens. The PCA plot data are 340 autosomal targets filtered for methylation β variance > 0.5 among the 44 samples. **C,** number of significant array target hyper- and hypomethylations as a function of tumor *SDH* mutation status (group delta β > 0.1 and $P < 0.05$). There are substantially more target hypermethylations in both *SDH*-mutant GIST and pgl/pheo compared with wild-type counterparts. **D,** 2-D hierarchical clustering of the 306 significant DMT between *SDH*-mutant pgl/pheo and adrenal reference (group delta β > 0.1 and p < 0.05). **E,** 2-D hierarchical clustering of the 303 significant DMT between *SDH*-wild-type pgl/pheo and adrenal reference (group delta β > 0.1 and $P < 0.05$). **F,** hierarchical clustering of 20 *SDH*-

mutant pgl/pheo, 9 wild-type pgl/pheo, and 15 reference baseline adrenal samples based on the 340 union targets from **D** and **E**. mut, mutant; wt, wild-type.

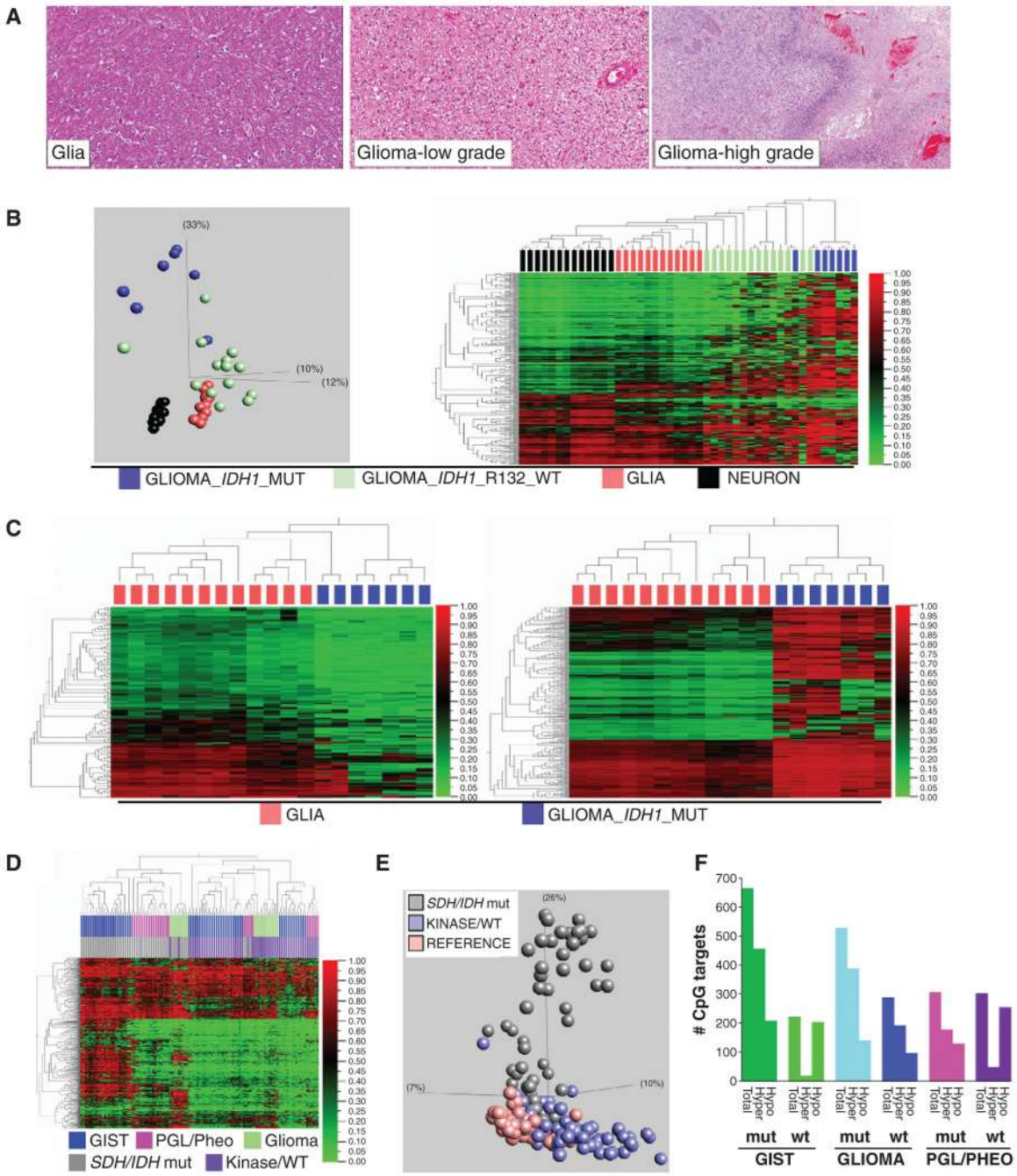

Figure 4.

Comparison of isocitrate dehydrogenase (*IDH*)-mutant glioma with *SDH*-mutant GIST. **A,** histomorphology of high-grade glioma, low-grade glioma, and comparison reference glial tissue. (Reference neuronal tissue is previously shown in Fig. 1A.) **B,** left, PCA segregates glial neoplasms according to oncogenotype, and reveals greater divergence from baseline glia for *IDH* mutants. The plot includes 7 *IDH1*-mutant glial tumors, 20 *IDH*-wt glial tumors, and 12 glia and 13 neuronal reference tissues. The PCA plot data are 386 autosomal targets filtered for methylation β variance > 0.5 among the 46 samples (GoldenGate

methylation data). Right: Unsupervised 2-D hierarchical clustering of the same data. **C,** left, hypomethylated DMT (group delta β > 0.1 and $P < 0.05$, $n = 140$ targets) identified in *IDH*-mutant glioma relative to reference glial tissue. Right, hypermethylated DMT (group delta β > 0.1 and $P < 0.05$, $n = 388$ targets) identified in *IDH*-mutant glioma relative to reference glial tissue (GoldenGate methylation data). **D,** unsupervised hierarchical clustering of all tumors in the study. Top colorbar: tumor type; bottom colorbar: oncogenotype. The *y*-axis data are 575 autosomal targets filtered for methylation β variance > 0.5 among the 113 samples. Oncogenotype drives higher level segregation. Also evident is the marked hypermethylation of *SDH/IDH*-mutant tumors of different lineage and anatomic sites. **E,** unsupervised PCA plot of 186 study samples annotated as normal tissue, *SDH/IDH*-mutant tumor, or *SDH/IDH*-wt/kinase-mutant tumor (var 0.5, 649 targets). **F,** quantities of significant hyper- and hypomethylated DMT in different tumor lineages as a function of mutant versus wt *SDH/IDH* status. mut, mutant; wt, wild-type.